
Article:
Lloyd-Laney, Henry O., Robinson, Martin J., Parkin, Alison orcid.org/0000-0003-4715-7200 et al. (1 more author) (2022) Theoretical assessment of the impact of noise on heuristic parameter inference methods for surface-confined non-catalytic voltammetry experiments. JOURNAL OF ELECTROANALYTICAL CHEMISTRY. 115927. ISSN 0022-0728

https://doi.org/10.1016/j.jelechem.2021.115927

Theoretical assessment of the impact of noise on heuristic parameter inference methods for surface-confined non-catalytic voltammetry experiments

Henry O. Lloyd-Laney,[†] Martin J. Robinson,[†] Alison Parkin,[*,‡] and David J. Gavaghan[*,†]

[†]*Department of Computer Science, University of Oxford, Wolfson Building, Parks Road, Oxford, OX1 3QD United Kingdom*

[‡]*Department of Chemistry, University of York, Heslington, York, YO10 5DD, United Kingdom*

E-mail: alison.parkin@york.ac.uk; david.gavaghan@dtc.ox.ac.uk

Abstract

When analysing a voltammetric experiment, the goal is often to obtain an estimate of parameter values — as defined by models which predict the current obtained by applying a time-varying potential input to an electroactive species under investigation. There are a variety of methods used to obtain these estimates, such as the heuristic approach, which involves extracting some feature from one or multiple voltammetry experiments, and obtaining an estimate of one or two parameters by analysing the extracted feature(s). In this paper we simulate voltammetry data using pre-defined parameter values for a purely Faradaic

surface-confined redox process, and then attempt to recover these values in the presence of varying amounts of synthetically-added noise, using both heuristic methods and a Bayesian inference approach. We show that the Bayesian approach recovers the true parameter values with either a greater or equivalent level of accuracy when compared to the heuristic approach, depending on the form of the data analysed. We show that the loss of accuracy for the heuristic case is primarily driven by the discarding of large amounts of data during the feature-extraction process.

Introduction

Voltammetry is a field with a strong numerical underpinning; analysis of data generated by a voltammetric experiment is almost universally informed by mathematical models describing the current response to the given potential input.[1,2] Examples of such models include the Butler-Volmer (BV) or Marcus-Hush relationships in the case of electron-transfer reactions.[3] Parameters contained within these models relate to fundamental properties of the redox-active species under investigation; for the BV case (which we use to generate the results in this paper), the reversible potential E^0 is a description of the thermodynamics of the reaction, and the rate constant k_0 the kinetics. Consequently, a large part of analysis of electrochemical data is an attempt to infer the values of such parameters. For the experimentalist, there is a large array of inference approaches to choose from. One such method is to use simulations of the total current — by systematically altering the parameters, the analyst aims to find a set of parameters that produce a simulation that is a good fit to the data, with this process taking place either on a manual or an automatic basis.[4,5] An alternative, which we analyse in this paper, is to extract some feature from the current data, often as a function of varying experimental conditions, such that the extracted feature has a predictable relationship to one or two parameters of interest. We consider how these methods are affected by the presence of independent and identically-distributed (i.i.d.) noise, the simplest form of noise model, in

the most ideal of cases — purely Faradaic current with no capacitance or dispersion in the thermodynamic or kinetic parameters,[6] for a single-electron surface-confined redox process with no catalytic activity. We have adopted this approach for simplicity, but it should be noted that there is extensive interest in the literature in systems with catalytic activity.[7–9] For a surface-confined species, the Faradaic current I_f is defined as

$$I_f = FA\Gamma\frac{d\theta}{dt} = FA\Gamma\bigg((1-\theta)k_{ox}(E) - \theta k_{red}(E)\bigg), \tag{1}$$

where F is Faraday's constant, A is the electrode surface area, Γ the surface coverage of the electroactive species, θ the proportion of the species which is oxidised, and the potential-dependant rate constants k_{ox} and k_{red}. These are expressed using the Butler-Volmer equations

$$k_{red}(E) = k^0 \exp\left(\frac{-\alpha F}{RT}(E - E^{0'})\right), \tag{2}$$

$$k_{ox}(E) = k^0 \exp\left(\frac{(1-\alpha) F}{RT}(E - E^{0'})\right), \tag{3}$$

such that k^0 is a potential-independent rate constant, α is symmetry factor, R the ideal gas constant and $E^{0'}$ is the reversible potential. Feature relationships can be experimentally[10,11] or analytically[3] derived, and are used as an alternative to total current analysis for a number of reasons. One such reason is ease of analysis, as the derived relationships are often mathematically simpler than the necessary simulation procedures for predicting the total current. They often take the form of a linear relationship between the extracted feature and a dependent variable, and consequently calculating the gradient or intercept of the line of best fit is all that is required to obtain a value for a parameter of interest; a process that can be trivially implemented in spreadsheet software such as excel. Another reason is that often the total experimental current contains non-idealities such as dispersion and non-linear capacitance that would require additional considerations to incorporate into a model of the total current, but that have a small effect on the extracted feature. Additionally, in the past

when performing large numbers of total current simulations was computationally infeasible, these approaches were far more achievable on available hardware. In this paper we quantify the impact of adding varying amounts of noise when attempting to perform one of 5 different inference techniques from the literature, two using direct current or cyclic voltammetry (DCV) and three using square wave voltammetry (SWV). We compare these results to an automatic approach which analyses either the same set of extracted features or the total current, and allows us to quantify the level of uncertainty inherent to either approach.

Approach

Heuristic inference

In order to determine the robustness of the various inference processes described below to the presence of i.i.d. noise, we generated multiple noisy voltammograms, using the simulation procedures for DCV and SWV described in our previous work,[6] and an excellent textbook on square wave voltammetry by Lovrić and coauthors respectively.[12] Noise was subsequently added using the process described in the "Noise" section. We then applied the various inference techniques to attempt to recover the appropriate parameter used in the simulation of the synthetic voltammogram. This process involves extracting some feature(s) from the synthetic current, or set of synthetic currents, and using those features to determine the value of the appropriate parameter. This value was recorded for each attempt, and the set of inferred parameters was used to assess the robustness of the technique. The parameters used for the simulation of the synthetic voltammograms can be found in table S1 and S2 for the DCV and SWV cases respectively, along with information about the number of features, and simulation times. Simulation parameters were chosen to be in a regime where the corresponding heuristic inference approach was maximally effective.

Markov-chain Monte Carlo

To benchmark the robustness of the various inference approaches, we compare the range of values obtained using our heuristic inference approach to the appropriate inferred parameter distribution obtained by an alternative statistical methodology, Bayesian inference, using a Markov-chain Monte Carlo (MCMC) algorithm. We have published previously on using MCMC methods in an electrochemical context, including a comprehensive review by Gavaghan et al.[1] The purpose of the MCMC algorithm is to sample from the posterior distribution, a distribution of parameters that best describe the observed data. At each iteration of the algorithm, a set of parameters is proposed and used to generate a simulation. This simulation is then compared to the observed data to calculate a likelihood. The value of this likelihood is then compared to the current best-likelihood, and the proposed parameters are accepted or rejected accordingly. By recording a history of the parameter vectors that were accepted, we obtain a distribution of likely values. A more fulsome discussion of this can be found in the supplementary information. The distributions generated by this process are not exactly comparable to the process of benchmarking the inference methods described in the previous section, since with the MCMC algorithms we only analyse one noisy set of data. However, if we were to repeat the MCMC process multiple times, it would not significantly alter the inferred parameter distributions (as the level of noise would be the same).

As long as we are consistent with how the parameters are used to generate a given simulation, it is possible to perform inference on either the total current from a single voltammogram, or the extracted features used for the heuristic approaches. This allows us to obtain both an explicit comparison between the MCMC and heuristic approaches (when fitting to sampled features) and allows us to observe the impact of feature extraction (by performing MCMC on the total current from a single voltammogram).

Noise

When creating artificially noisy voltammograms, our procedure for the addition of i.i.d. noise is simply

$$I_{noisy}(t) = I_{sim}(t) + \epsilon(t), \quad \epsilon(t) \sim \mathcal{N}(0, \max(I_{sim})p), \tag{4}$$

such that $\mathcal{N}(0, \max(I_{sim})p)$ indicates a normally-distributed random variable with 0 mean, and a standard deviation proportional $\max(I_{sim})$, and p is a scaling factor in the range of 0.005-0.05, or 0.5-5% of the maximum. We have found that a noise level of 0.5% of the maximum current is usually a good approximation to the noise observed in actual experimental voltammetry data.[13]

Heuristic inference approaches

DCV

DCV is one of the simplest and most widely used voltammetry techniques. A single DCV experiment uses a potential input that increases or decreases linearly (i.e. with a constant potential scan rate) to a switching potential, and then returns to the starting potential.

Surface coverage

The surface coverage parameter Γ can be determined from the area under either the reductive or oxidative peak, such that, for a purely Faradaic current beginning at time $t = 0$ and ending at time $t = t_N$, where F is Faraday's constant, i_f is the total Faradaic current, n the number of electrons transferred, v is the scan rate and a the electrode area[3]

$$FAnv\Gamma = \int_0^{t_N} i_f \tag{5}$$

In practice, the integral in equation 5 is calculated using numerical quadrature, for example by using Simpson's rule.[3] An example of this process is shown graphically in figure 1

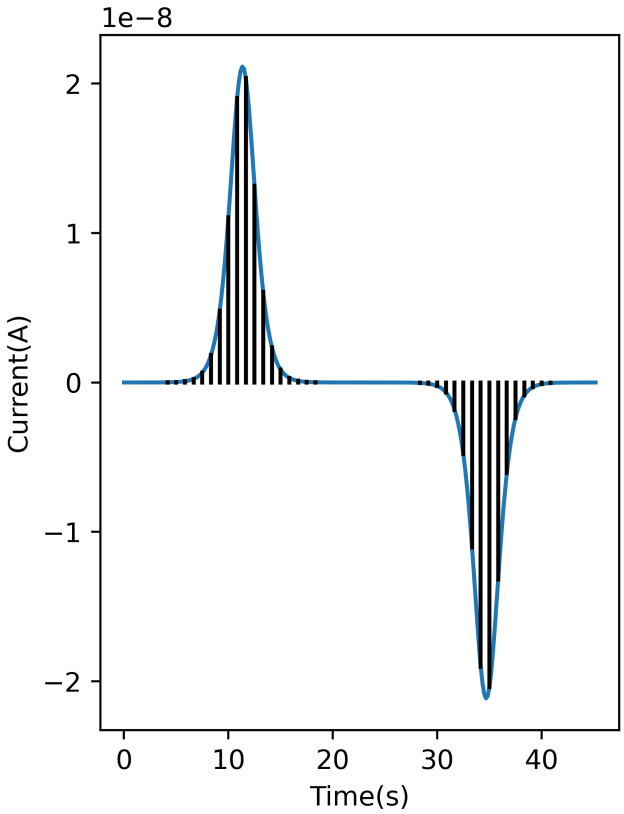

Figure 1: Purely Fardaic DCV experiment vs. time, with black lines indicating how the integral is approximated using numerical quadrature

Rate constant

Trumpet plots, where multiple DCV experiments are performed at different scan rates and the potential position $E_p(ox)/E_p(red)$ of the peak current is recorded, can be used to determine the rate constant k_0. These plots are popular as the relationship between the peak position and the scan rate is not affected by background currents arising from double-layer capacitance to the same extent as the rest of the voltammogram. Consequently, analysis of the trumpet plot is less dependent on the ability to correctly subtract away background current. By rearranging the Butler-Volmer equations, we obtain an expression for the potential

of the oxidative/reductive peak as a function of the logarithm of the scan rate $\ln(v)$ and k_0, such that

$$E_{p(ox)} - E^0 = -\frac{RT}{\alpha nF}\ln(v) - \frac{RT}{\alpha nF}\ln\left(\frac{\alpha nF}{RTk_0}\right), \tag{6}$$

and

$$E_{p(red)} - E^0 = \frac{RT}{(1-\alpha)nF}\ln(v) + \frac{RT}{(1-\alpha)nF}\ln\left(\frac{(1-\alpha)nF}{RTk_0}\right), \tag{7}$$

where F is Farday's constant, T is the temperature, R the ideal gas constant and n the number of electrons. A linear function of the form $f(x) = mx + c$ can consequently be fit to the the linear regions of an appropriately normalised trumpet plot, which represents $E_{p(ox/red)} - E^0$ as a function of $\ln(v)$, as shown on the left hand plot of figure 2. Consequently, the recovered gradient m can be used to calculate the value of α, and subsequently the recovered intercept c can be used to determine the value of k_0.[3]

SWV

Square-wave voltammetry uses a square-wave potential superimposed over a staircase potential — jumps between potential values are hypothetically instantaneous, and the potential is then maintained at a constant value until the subsequent jump. The current is sampled at the end of each pulse, and this sampling is separated into "forwards current", where the sampling occurs at the maximum of each square-wave oscillation, "backwards current" which is sampled at the minimum, and the net current, which is simply the backwards current subtracted from the forwards.[12] The sampling procedure is shown graphically in the supplementary information in figure S1.

A note on noise in square-wave voltammetry

Initially, when generating noisy SW voltammograms, we used the magnitude of the total current (as opposed to the sampled) to calculate the level of noise. In other voltammetric experiments, the magnitude of the current arising from the signal to be analysed (in DCV,

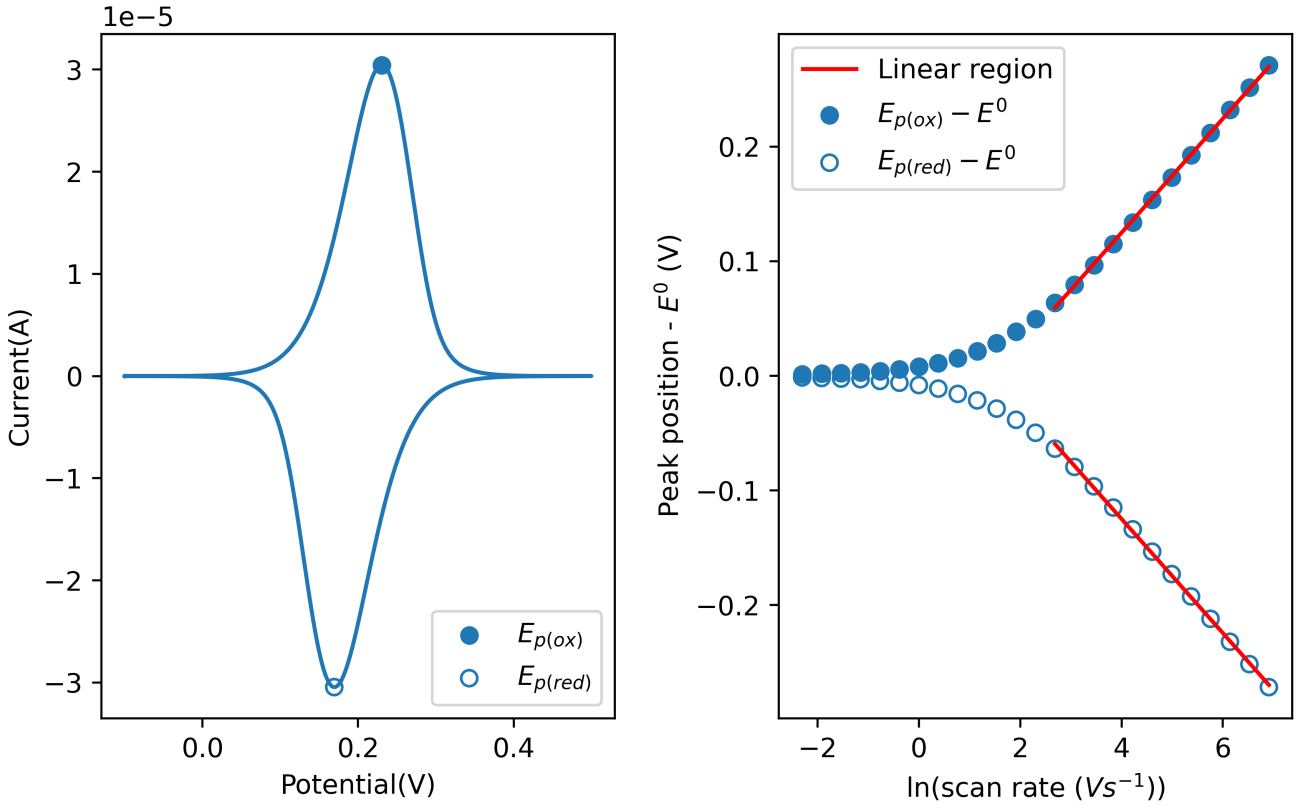

Figure 2: Left: Purely Faradaic DCV current vs. potential, where $v = 5\ Vs^{-1}$ and $k_0 = 100\ s^{-1}$. Right: Trumpet plot showing normalised peak positions of oxidative and reductive peaks, and the linear region through which we draw a line of best-fit (red)

for example, the reductive and oxidative peaks) is usually on a similar order of magnitude as the value of the maximum current. In the case of SWV, the current is sampled at the end of a pulse, which is effectively the *minimum* magnitude of the current on the timescale of that pulse. Consequently, any set of parameters generates a current which contains a large discrepancy between the maximum total current and the average magnitude of the sampled current will result in a magnitude of ϵ in equation 4 that is sufficient to obscure any signal observed in the sampled current, sometimes two or three orders of magnitude larger. As the impact of noise does not seem to be a particularly high concern among SWV practitioners, and after observation of real SWV data, we have decided, for the purposes of this exercise, to use the maximum of the sampled SWV net current rather than the maximum of the total

current to calculate the noise value.

Reversible rate constants

At sufficiently high values of K (i.e. the dimensionless kinetic parameter $\frac{k_0}{f}$, where f is the square-wave frequency) for a surface-confined redox process interrogated using a square-wave potential, a phenomenon known as "peak-splitting" is observed, which refers to the sampled net current exhibiting two distinct peaks. Lovric et. al determined that the separation between these two peaks (ΔE_p) was a function of the square wave amplitude in mV (E_{sw}) and K, such that $\Delta E_p = 5\frac{k_0}{f} + 2nE_{sw} - 50mV$.[10] This expression can be rearranged into the form $y = mx + c$, such that $mx = \frac{k_0}{f}$, and consequently the value of k_0 can be determined from the fitted value of m.

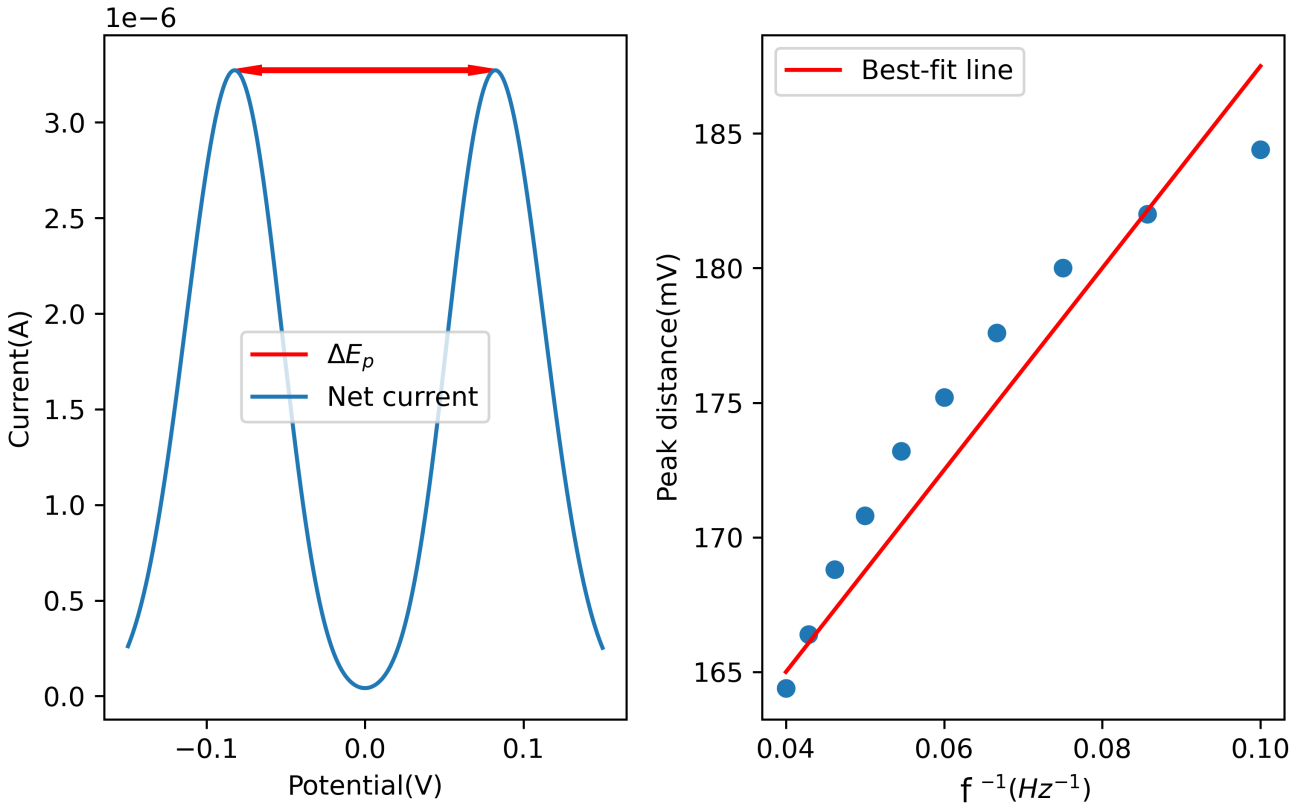

Figure 3: Left: net SWV current, generated using $f = 25$ Hz and $k_0 = 75\ s^{-1}$, with the peak distance metric shown in red. Right: Normalised peak distances plotted as a function of the inverse frequency (blue dots), with the best-fit line used to calculate k_0 shown in red.

Symmetry factor

In the same paper, Lovric et. al also describe a method to obtain an estimate of the symmetry factor α, with similar assumptions about the value of $\frac{k_0}{f}$, by calculating the ratio of the two peak heights, such that

$$\alpha = -\frac{1}{3.4606} \ln\left(\frac{|I_f|}{5.614|I_b|}\right), \tag{8}$$

where I_f and I_b are the maximum currents for the sampled forwards and backwards SWV currents respectively.[10] The process of obtaining I_f and I_b is shown on the left hand side of figure 4. The right hand shows the value of alpha calculated from SW voltammograms simulated with differing values of α (and a $\frac{k_0}{f}$ value of 6), along with the predictions from equation 8, indicating very good agreement

Quasi-reversible rate constants

The peak-splitting inference approach for k_0 is only valid under conditions where peak-splitting is observed, i.e. $\frac{k_0}{f} > 2$. Compton and coauthors described an approach for determining the rate constant when $0.01 < \frac{k_0}{f} < 0.5$. They termed this approach the "quasi-reversible maximum". Multiple SW voltammograms are measured at varying frequencies f and amplitudes E_{sw}. For each experiment, the peak net current, normalised by E_{sw} is noted. The maximum of these maxima I_{QRM} is recorded as a function of frequency, which is then used to determine k_0 using the following relationship[11]

$$\frac{k_0}{f} = 10^{\frac{I_{QRM}-0.8}{-148.08}}. \tag{9}$$

As before, we determine the gradient m of the normalised I_{QRM} values vs. the inverse frequency, giving us a value for k_0. This process is shown in figure 5.

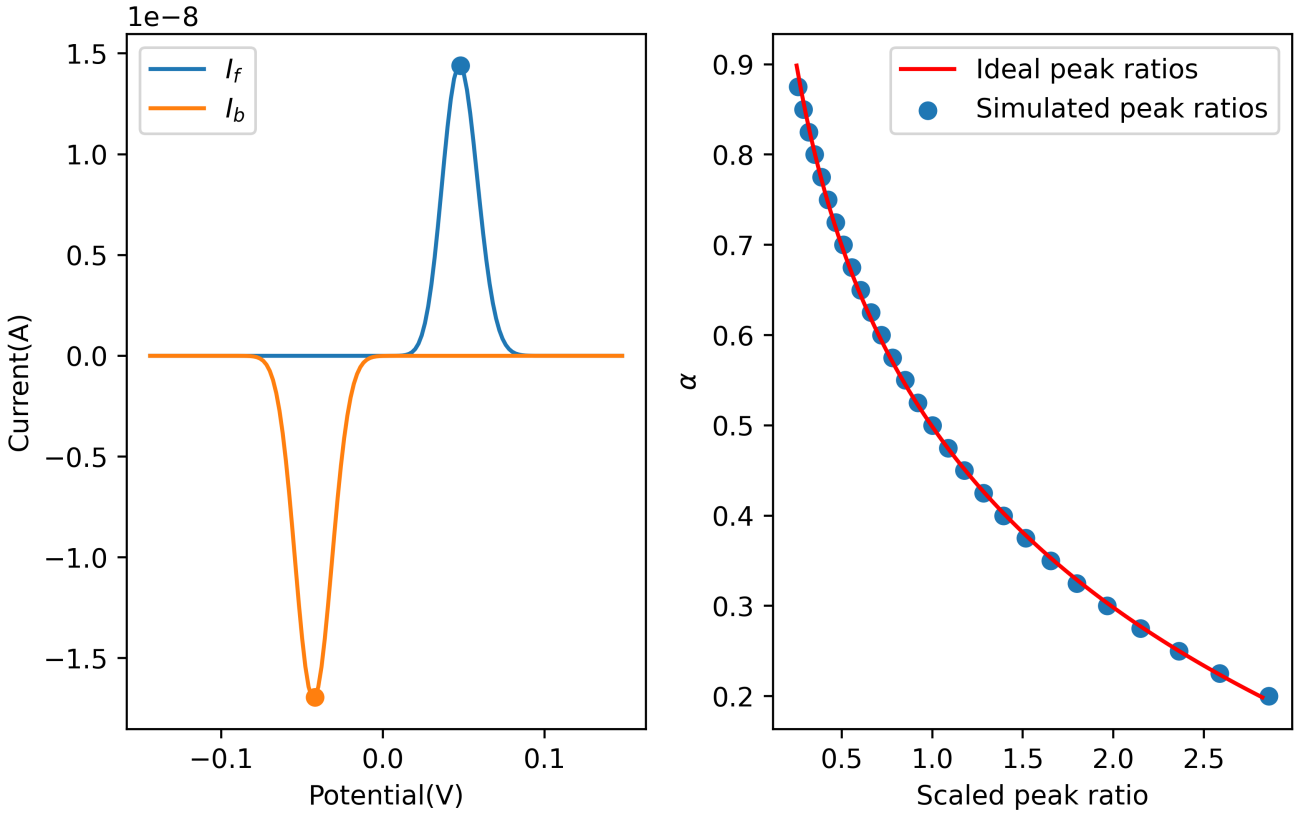

Figure 4: Left: Forward and backward currents from a SWV experiment $f = 1$ Hz, $k_0 = 6$ s^{-1} and $\alpha = 0.5$, with the key features I_f and I_b indicated. Right: Peak ratios obtained from sampled current simulated with different values of α vs the values of α calculated using equation 8 (blue) and "ideal" peak ratios calculated by rearranging equation 8 (red)

Results and Discussion

DCV: Surface coverage

The first heuristic method, inferring the surface coverage in a surface-linked DCV experiment by determining the area under the oxidative and reductive peaks, was extremely robust to the addition of I.I.D. noise. This can be observed in figure 6 and in table 1, where even with 5% noise, the standard deviation of inferred Γ values is less that 1% of the true value. This can be explained by the fact that, because the mean of the noise in equation 4 is 0, the overall impact on the area under the curve of the current is minimal, leading to the very accurate estimates observed. Because of this accuracy, we did not believe it was necessary to

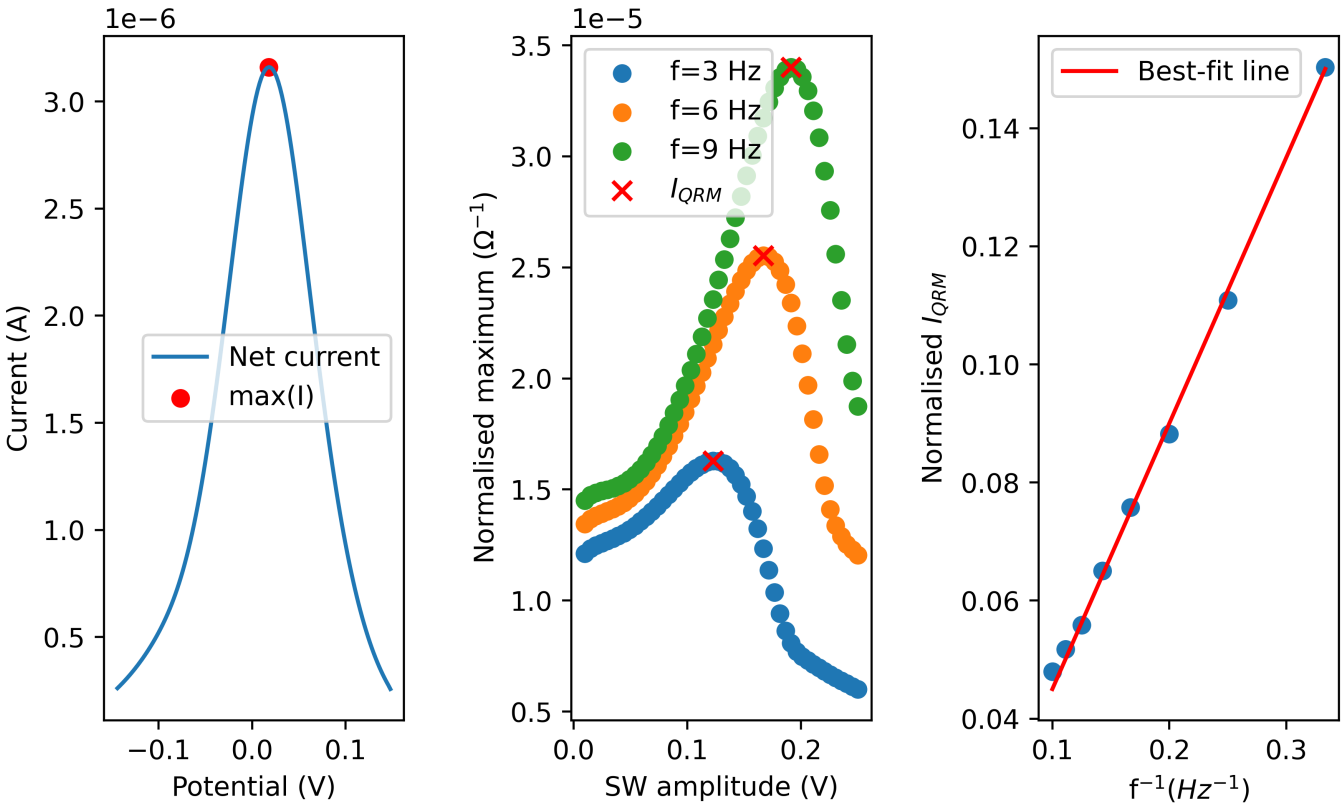

Figure 5: Left: Net SWV current, simulated using $f = 7$ Hz, $k_0 = 0.5\ s^{-1}$ and $E_{sw} = 0.13\ V$, with the maximum current indicated by the red dot. Centre: maximum current (normalised by the value of E_{sw}), plotted against the varying E_{sw} value for three different frequencies. The I_{QRM} value is indicated by the red cross. Right: I_{QRM} plotted as a function of the inverse frequency, with the best-fit line drawn in red.

compare this technique to MCMC. Although it is outside of the scope of the paper (which focuses on the impact of i.i.d. noise), we should note that this heuristic is highly impacted by the efficacy with which the background current is subtracted. In figure 6, and all subsequent histograms, "frequency" refers to the number of samples of that parameter value returned by the MCMC algorithm, explained in more detail in the SI.

DCV: Kinetic parameter

The method of inferring the kinetic parameter from trumpet plots was by far the least robust to the presence of i.i.d. noise of all the techniques assessed. The spread of values, as

Table 1: Ratio of the standard deviation of the inferred parameter values for each inference approach to the true value of that parameter, with varying amounts of added noise. Where appropriate, the values in brackets were inferred from fitting to the total current, and the other values are from fitting to the extracted features.

Method	Noise level	DCV Γ	DCV k_0	SWV k_0 (R)	SWV α	SWV k_0 (QR)
Heuristic	0.5%	0.06%	4.04%	1.99%	0.28%	1.73%
	1%	0.13%	5.8%	2.88%	0.51%	2.23%
	2%	0.26%	7.98%	3.82%	0.98%	2.9%
	3%	0.38%	9.83%	4.67%	1.33%	3.65%
	4%	0.5%	13.25%	5.39%	1.68%	4.1%
	5%	0.64%	15.95%	5.8%	2.14%	4.51%
MCMC	0.5%	N/A	0.97%(0.05%)	3.26%(0.02%)	N/A(0.12)%	2.74%(0.05%)
	1%		1.2%(0.11%)	2.97%(0.04%)	N/A(0.24)%	3.64%%(0.11%)
	2%		1.83%(0.22%)	3.43%(0.07%)	N/A(0.51)%	2.55%(0.18%)
	3%		2.41%(0.32%)	3.73%(0.11%)	N/A(0.73)%	3.86%(0.27%)
	4%		2.3%(0.43%)	4.06%(0.16%)	N/A(1.1)%	4.32%(0.4%)
	5%		2.68%(0.55%)	4.13%(0.18%)	N/A(1.17)%	6.33%(0.52%)

communicated in table 1, and shown in figure 7 is 4-8 times worse than when using MCMC using the same (peak-position) observations, and 1-2 orders of magnitude worse when fitting to the total current. We believe that the reason for the poor performance of this method is that it requires accurate estimates of both the intercept and gradient of the best-fit line, as opposed to the peak-splitting and quasi-reversible maximum methods (discussed below) that only require an estimate of the gradient. As the method requires normalisation of the peak potentials using the reversible potential, we also assessed the impact of incorrect estimates of E^0, but found that it did not significantly alter the results presented in table 1 and figure 7.

SWV: Kinetic parameter, reversible case

The performance of the MCMC algorithm when fitting to ΔE_p recovers values with an accuracy that has the same order of magnitude as the heuristic approach, although it is more affected relative to the heuristic approach at the lower noise percentages, but less affected at the higher percentages. This may reflect the fact that the majority of the uncertainty in this

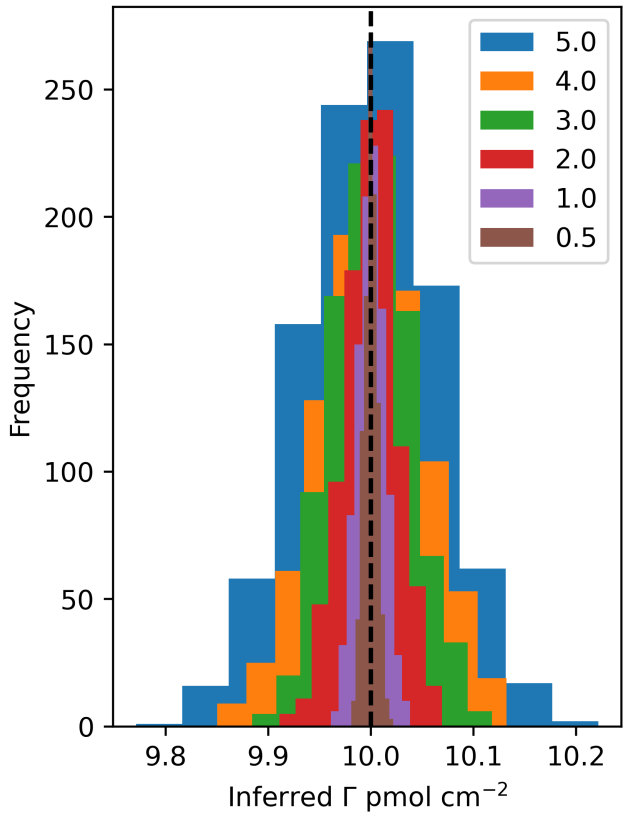

Figure 6: Values of the surface coverage parameter Γ, where the true value was 10 pmol cm^{-2}, inferred using the approach described in the heuristic section, with varying amounts of noise. The noise percentage is indicated in the legend. We did not compare the results of this to MCMC in this case, because the values inferred by this method were so close to the true value.

approach is driven by the amount of information that is discarded at the feature extraction stage (i.e. the representation of a SWV experiment as a single ΔE_p value). This is reinforced by the fact that the values inferred when analysing a single SWV experiment using MCMC have a spread around the true value that is $\sim 1-2$ orders of magnitude smaller, as shown in figure 8.

SWV: Symmetry factor

The method of estimating α from the ratio of peak heights present in the net SWV current was the second most effective heuristic approach when judged by having the smallest range

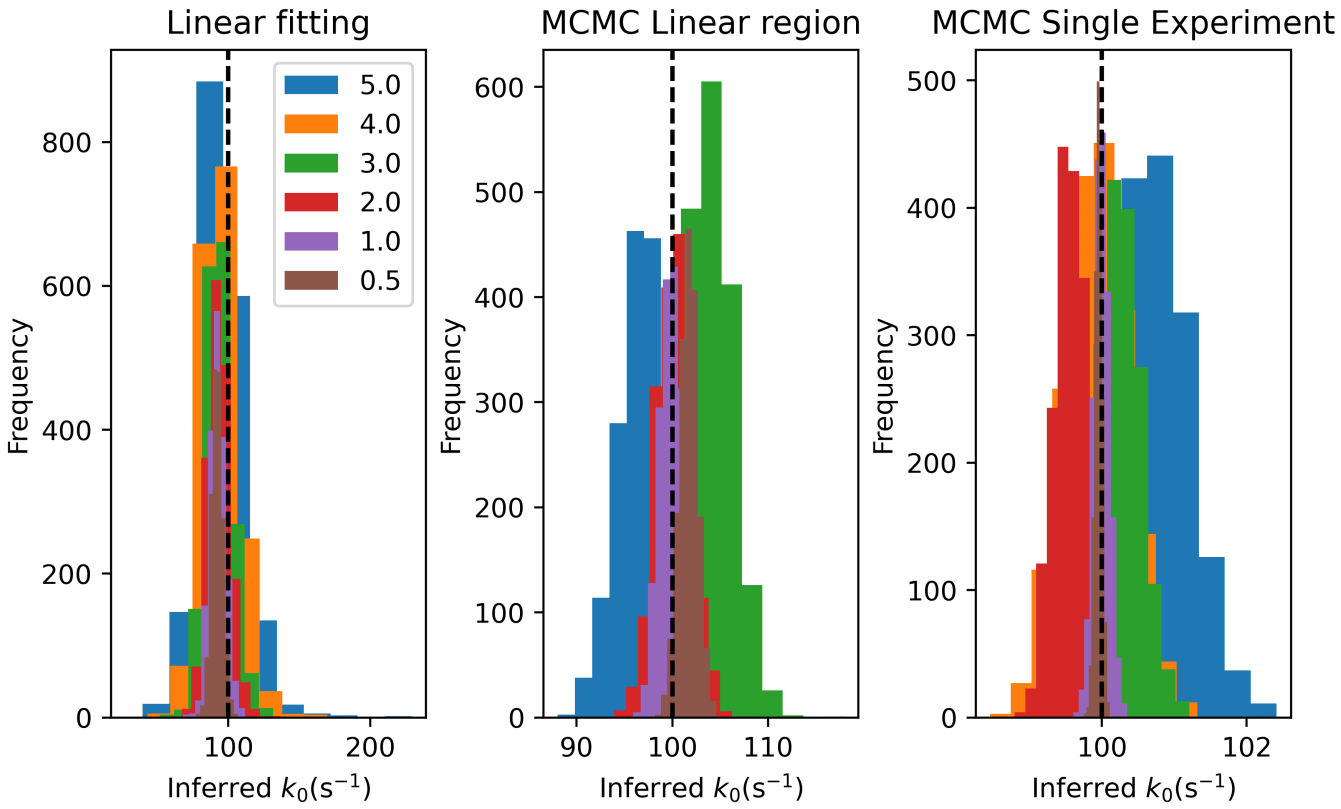

Figure 7: Left and centre: Kinetic parameter values inferred by fitting to the linear region of a trumpet plot for varying amounts of noise, where the noise percentage is indicated by the legend, and the true value of k_0 was $100s^{-1}$. For the linear fitting, the inferred anodic and cathodic values were pooled. Right: Inferred parameter values for k_0 using MCMC, fitted to a trumpet plot.

of inferred values around the true parameter, with the spread being only 2-3 times larger than for the MCMC case, as observed in figure 9. We did not use MCMC on the peak ratio data, as this would have required fitting to a single datapoint, which is not appropriate for MCMC.

SWV: Kinetic parameter, irreversible case

As with the peak-splitting case, the performance of the heuristic approach and MCMC when applied to the heuristic features is of a similar order of magnitude, with the values inferred using the total current analysed by MCMC being 1-2 orders of magnitude more accurate, as

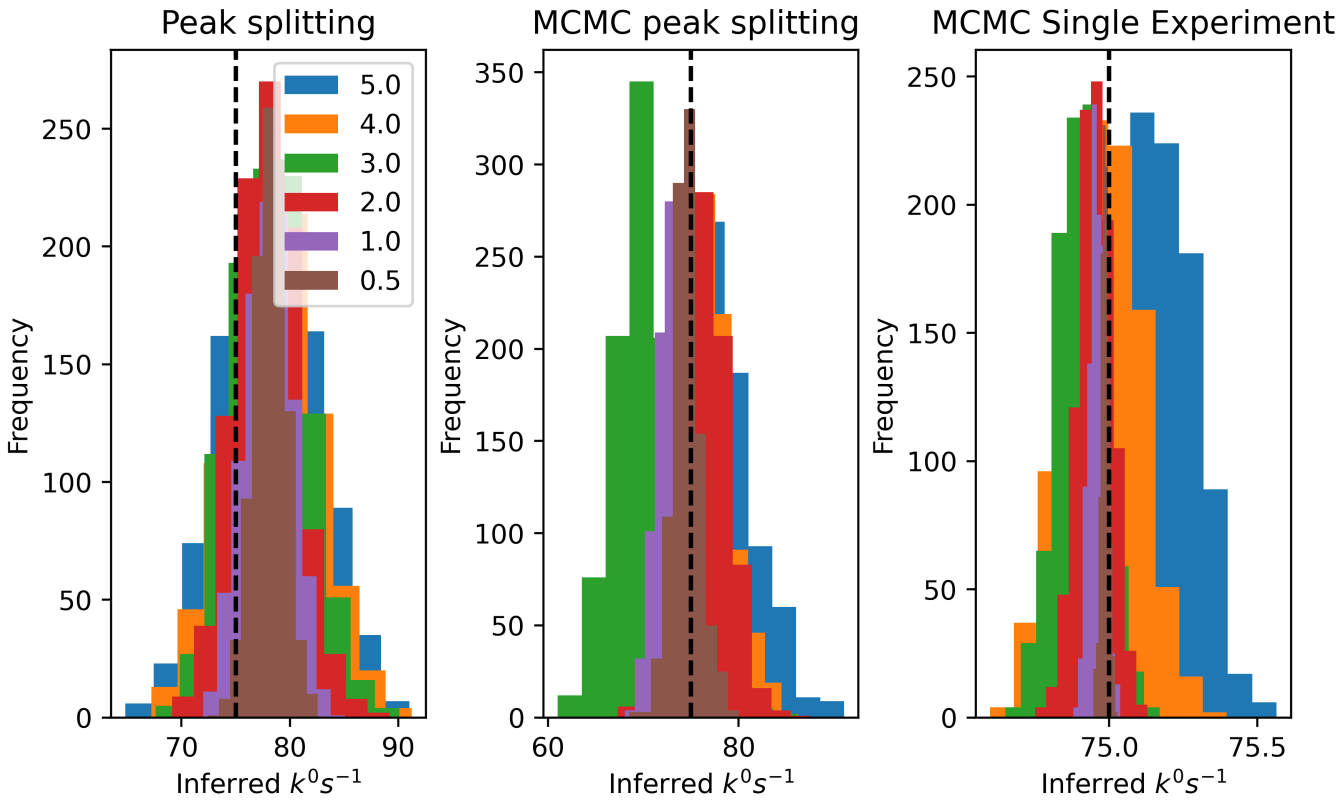

Figure 8: Left: Values of the kinetic parameter inferred from the net sampled SWV current using the peak splitting method described in the heuristic inference section, for varying amounts of noise where the noise percentage is shown in the legend. The true value of k_0 was 75s^{-1}. Centre and right: Values of the kinetic parameter inferred using MCMC, using sampled net current (centre) and total current (right).

shown in figure 10.

Conclusions

These results indicate that, under the conditions analysed here, methods which involve the extraction of features from the total current are outperformed by analysing the total current. The worst-performing heuristic method, using the linear region of a trumpet plot, performs worse than both fitting to the total current and fitting to the extracted features, presumably because it requires accurate estimates of both the gradient and intercept of the fitted line. The approach with the best accuracy (DCV surface coverage) did not use a linear

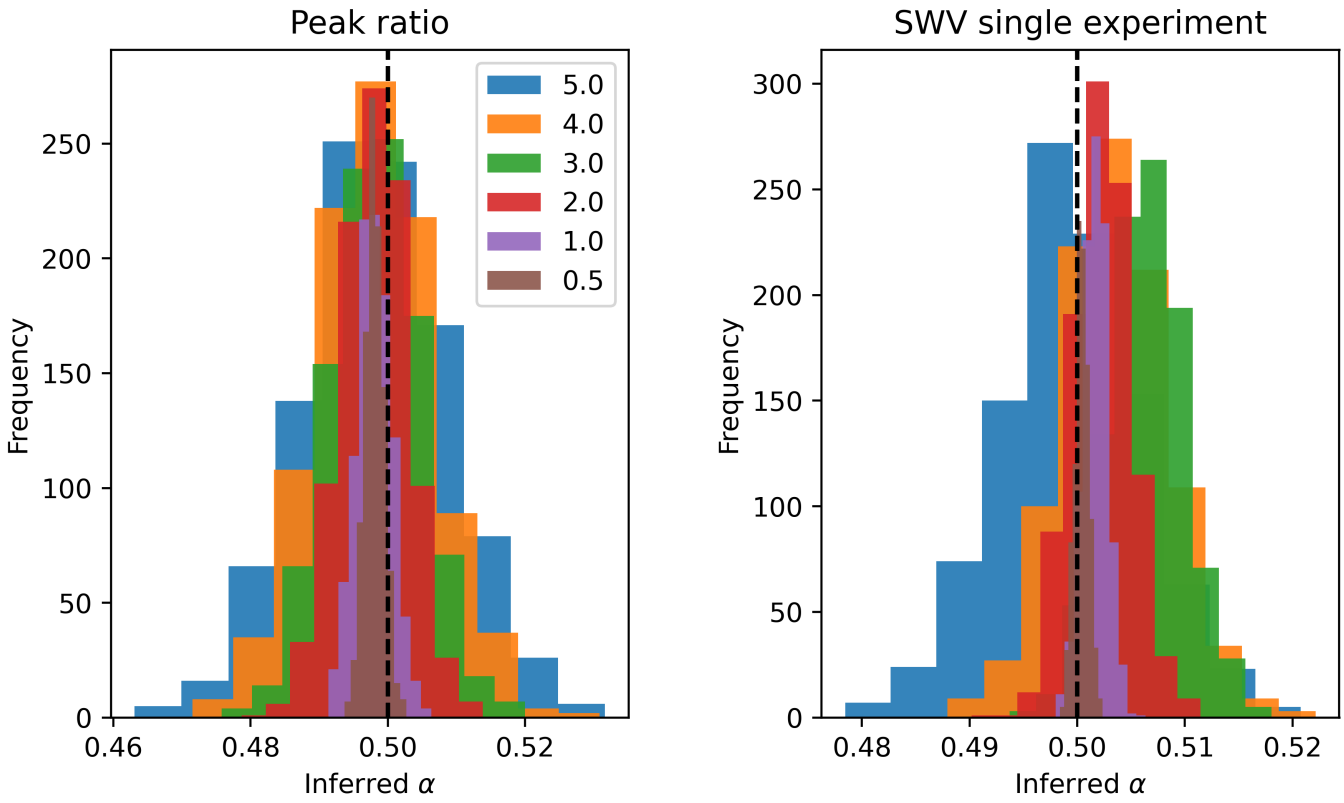

Figure 9: Left: α values inferred from noisy sampled forwards and backwards SWV currents using the peak ratio approach described in the heuristic inference section, for different values of noise, where the noise percentage is shown in the legend. The true value of α was 0.5. Right and centre: α values inferred from noisy sampled net current (centre) and total SWV current (right)

fit at all. The analysis of SWV data is more interesting - the performance of the heuristic approaches are comparable to the results obtained from using MCMC to fit to the same set of features, implying that the linear fitting (requiring only an estimate of the gradient) is as robust as the MCMC approach. In addition, when using MCMC to fit to features for the peak-splitting and QRM approaches, the standard deviation of the recovered values does not increase monotonically with the added noise (as it does with MCMC fitting to the total current) — these two observations suggest that the majority of the uncertainty with these techniques is driven by the feature extraction process, where information is discarded in order to compress a voltammetric experiment into a single data-point, rather than the

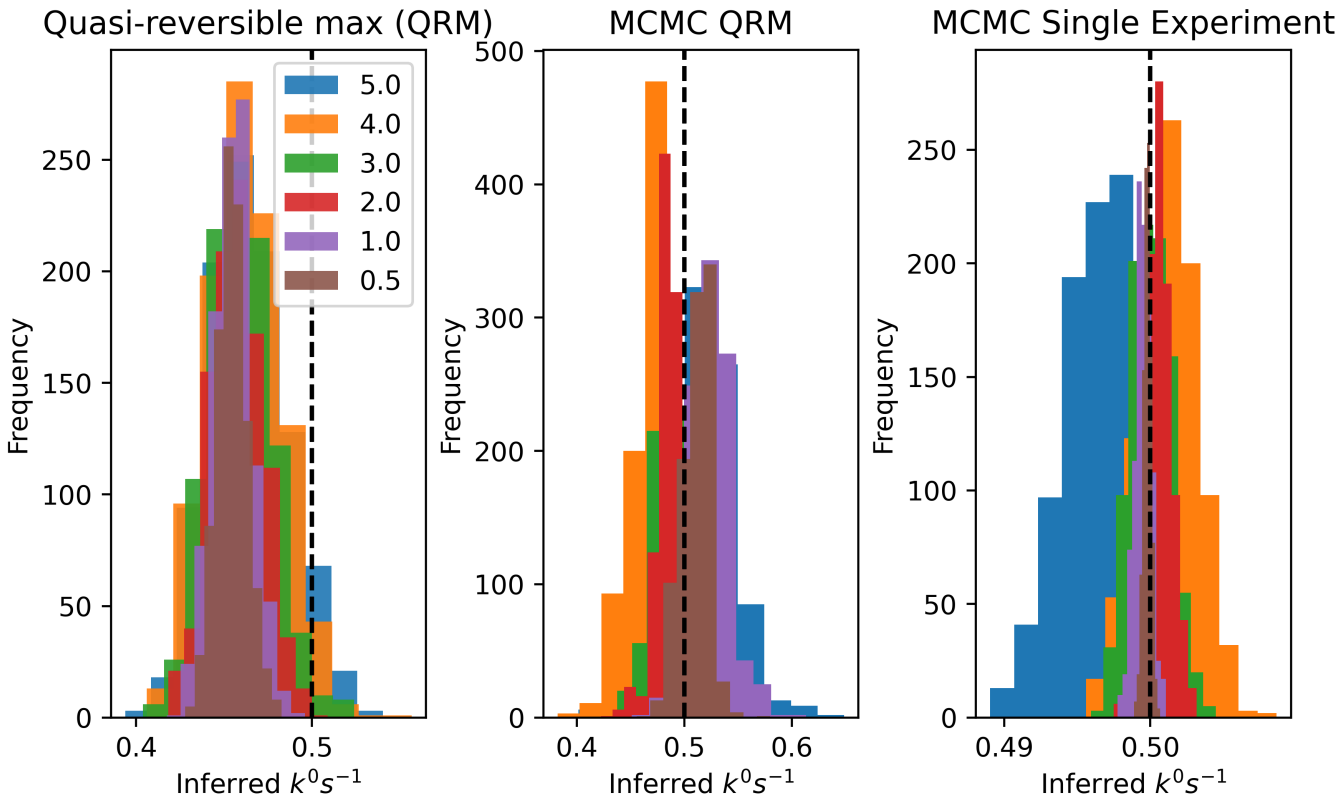

Figure 10: Left: Kinetic parameter values inferred from sampled net SWV current using the quasi-reversible maximum method, for different values of noise where the noise percentage is shown in the legend. The true value of k_0 was 0.5s^{-1}. Right and centre: Kinetic parameter values inferred using MCMC using noisy sampled (centre) and total (right) SWV current.

actual fitting process. Interestingly, increasing the number of extracted features for the peak splitting case from 20 (as used to generate the values in figure 8) to 70, which is consistent with the number of points in the sampled total current, reduced the width of the kinetic distribution inferred by MCMC analysis of ΔE_p, which is expected as this is increasing the amount of data "visible" to the MCMC. For the 0.5% noise case, the standard deviation of the inferred kinetic distribution decreased from 2.74% to 0.5% of the true value (of 75s^{-1}) as a result of this increase in the amount of data. However, this standard deviation obtained from fitting to the ΔE_p was still 10 times larger than the MCMC-inferred standard deviation of the kinetic parameter for the total current at 0.5%, which implies that the difference between the standard deviations of distributions inferred by fitting to extracted features vs.

total current using MCMC is not entirely due to a simple discrepancy in the number of observations. The remainder of the difference is due to the intrinsically greater information present in the total current relative to the extracted features. Additionally, as detailed in the SI, the assumption of i.i.d. noise for the heuristic case may lead to some biasing of the kinetic distribution away from the true value.

It should also be noted that the non-monotonic behaviour may be the result of inaccurate assumptions about the noise model, which we discuss in the supplementary information. Additionally, all simulation of synthetic current was performed in the absence of background current, and that the presence of the background current is one of the reasons discussed for using the feature extraction methods in the first place. However, even when fitting to the extracted features instead of the total current, MCMC methods at minimum offer similar levels of accuracy. This is in addition to their other advantages, in particular the ability to provide a measure of confidence for multiple parameters simultaneously, while the heuristic approach only returns a single estimate for one or two parameter values. Of the three reasons discussed for using the heuristic approach, namely ease of implementation, smaller impact from non-idealities and computational feasibility, only the second motivation is really valid, as it is becoming consistently easier to implement statistical approaches such as MCMC, and computing power is no longer a limiting factor. However, even in this case, the extracted features can still be analysed using an MCMC approach, rather than using a linear fit.

Acknowledgement

HOLL gratefully acknowledges funding from the EPSRC and BBSRC Centre for Doctoral Training in Synthetic Biology (grant EP/L016494/1). MJR and DJG gratefully acknowledge support from the EPSRC Centres for Doctoral Training Programme (EP/S024093/1).

References

(1) Gavaghan, D. J.; Cooper, J.; Daly, A. C.; Gill, C.; Gillow, K.; Robinson, M.; Simonov, A. N.; Zhang, J.; Bond, A. M. Use of Bayesian inference for parameter recovery in DC and AC Voltammetry. *ChemElectroChem* **2018**, *5*, 917–935.

(2) Bieniasz, L.; Speiser, B. Use of sensitivity analysis methods in the modelling of electrochemical transients: Part 3. Statistical error/uncertainty propagation in simulation and in nonlinear least-squares parameter estimation. *Journal of Electroanalytical Chemistry* **1998**, *458*, 209–229.

(3) Bard, A. J.; Faulkner, L. R., et al. Fundamentals and applications. *Electrochemical Methods* **2001**, *2*, 580–632.

(4) Adamson, H.; Bond, A. M.; Parkin, A. Probing biological redox chemistry with large amplitude Fourier transformed ac voltammetry. *Chemical Communications* **2017**, *53*, 9519–9533.

(5) Dauphin-Ducharme, P.; Arroyo-Currás, N.; Kurnik, M.; Ortega, G.; Li, H.; Plaxco, K. W. Simulation-based approach to determining electron transfer rates using square-wave voltammetry. *Langmuir* **2017**, *33*, 4407–4413.

(6) Lloyd-Laney, H. O.; Robinson, M. J.; Bond, A. M.; Parkin, A.; Gavaghan, D. J. A Spotter's guide to dispersion in non-catalytic surface-confined voltammetry experiments. *Journal of Electroanalytical Chemistry* **2021**, *894*, 115204.

(7) Gulaboski, R.; Mirčeski, V.; Lovrić, M. Square-wave protein-film voltammetry: new insights in the enzymatic electrode processes coupled with chemical reactions. *Journal of Solid State Electrochemistry* **2019**, *23*, 2493–2506.

(8) Gulaboski, R. Theoretical Contribution Towards Understanding Specific Behaviour of

"Simple" Protein-film Reactions in Square-wave Voltammetry. *Electroanalysis* **2019**, *31*, 545–553.

(9) Gulaboski, R.; Mirčeski, V.; Lovrić, M. Critical aspects in exploring time analysis for the voltammetric estimation of kinetic parameters of surface electrode mechanisms coupled with chemical reactions. *Macedonian Journal of Chemistry and Chemical Engineering* **2021**, *40*, 1–9.

(10) Mirčeski, V.; Lovrić, M. Split square-wave voltammograms of surface redox reactions. *Electroanalysis* **1997**, *9*, 1283–1287.

(11) Mirčeski, V.; Laborda, E.; Guziejewski, D.; Compton, R. G. New approach to electrode kinetic measurements in square-wave voltammetry: amplitude-based quasireversible maximum. *Analytical chemistry* **2013**, *85*, 5586–5594.

(12) Mirčeski, V.; Komorsky-Lovrić, Š.; Lovrić, M. In *Square-wave voltammetry: theory and application*; Scholz, F., Ed.; Springer Science & Business Media, 2007.

(13) Lloyd-Laney, H.; Robinson, M.; Parkin, A.; Gavaghan, D. Comparison of Numerical and Analytical Approaches for Simulating Purely Sinusoidal Voltammetry. *ChemRxiv* **2021**,